

promoting access to White Rose research papers



Universities of Leeds, Sheffield and York
<http://eprints.whiterose.ac.uk/>

This is an author produced version of a paper published in **Smart Materials and Structures**.

White Rose Research Online URL for this paper:
<http://eprints.whiterose.ac.uk/10239>

Published paper

Diaz, I.M., Reynolds, P. (2009) *Robust saturated control of human-induced floor vibrations via a proof-mass actuator*, Smart Materials and Structures, 18 (12), Art no.125024
<http://dx.doi.org/10.1088/0964-1726/18/12/125024>

Robust saturated control of human-induced floor vibrations via a proof-mass actuator

I M Díaz¹ and P Reynolds²

¹ Escuela Técnica Superior de Ingenieros Industriales, Universidad de Castilla-La Mancha, Edificio Politécnico, Av. Camilo José Cela s/n, 13071, Ciudad Real, Spain

² Department of Civil and Structural Engineering, The University of Sheffield, Sir Frederick Mappin Building, Mappin Street, Sheffield, S1 3JD, United Kingdom

E-mail: ivan.munoz@uclm.es and p.reynolds@sheffield.ac.uk

Abstract

This paper is concerned with the design of a robust active vibration control system that makes use of a proof-mass actuator for the mitigation of human-induced vibrations in floor structures. Ideally, velocity feedback control (VFC) is unconditionally stable and robust to spillover effects, interlacing of poles and zeros of collocated control is then accomplished. However, the use of a proof-mass actuator influences the system dynamics and the alternating pole-zero pattern of the system formed by the actuator and structure is no longer fulfilled. However, a controlled migration of the two zeros of the root locus plot at the origin, resulting from the acceleration output, can be achieved by adding a feed-through term (FTT) to the structure acceleration output. That is, the FTT enables to control the position of a pair of complex conjugate zeros (an anti-resonance in the frequency domain). This paper proposes the introduction of a FTT designed in such a way that the anti-resonance at the origin is located between the actuator resonance and the structure fundamental resonance. Hence, an integral controller leads to infinite gain margin and significant phase margin. Simulation and experimental results on a concrete slab strip have validated the proposed control strategy. Significant improvements in the stability properties compared with VFC are reported.

1. Introduction

The current trend towards lighter and slender structures with fewer non-structural elements has resulted in structures with less inherent damping and lower natural frequencies, which are more susceptible to excitation by human occupants. Examples of significant vibrations caused by human motions have been reported in numerous structures such as office buildings, footbridges and sport stadia, amongst others [1]. Such vibrations can cause a serviceability problem in terms of disturbing the users, but they do not often affect the safety of structures.

Several guidelines, such as [2,3], are available to take into consideration human-induced vibrations. Nonetheless, structures can still exhibit excessive vibration levels. With regards to floor structures, improvement is usually complicated and involves structural and non-structural changes and severe disruption of occupation. Another possibility is the use of tuned mass dampers [4] or semi-active tuned mass dampers [5] to add damping to the floor system. However, due to their passive nature, these systems are often ineffective for small vibration amplitudes (such as those produced by human loading) and several of these devices have to be used to achieve significant vibration reduction over multiple modes. In this case, an active vibration control (AVC) system might be more effective [6]. A state-of-the-art review of passive, semi-active and active systems for mitigation of human-induced vibrations can be found in [7]. Moreover, techniques to mitigate floor vibrations are reviewed in [8].

Even though AVC systems have gained some level of acceptance in civil engineering applications, there are still some issues to address, such as stability of these systems. Civil structures are by themselves stable and might be destabilized through the use of an AVC whereas other structures, like aerospace structures, require an AVC system for stabilization.

Techniques such as LQR, H_2 and H_∞ commonly appear in research work [9–11] and they are usually focused on cancelling hazardous vibrations due to earthquakes and winds. These techniques usually require complex design methodologies based on a system model that involves full state-space feedback resulting in control systems of high order and possible poor stability margins (which might result in spillover instabilities). Direct output measurement feedback control might be preferable in practical problems, since it is rarely possible to measure the system state [12].

One way to guarantee stability is the use of collocated actuator and sensor, commonly known as collocated control. Both of them are located physically at the same point on a structure and hence an interlacing pole-zero pattern is exhibited [13]. Then, a properly designed feedback compensator will allow the controlled system to be unconditionally stable and robust to spillover effects in the absence of actuator and sensor dynamics [14]. However, when these additional dynamics are considered, the interlacing property is no longer accomplished and the stability of the controlled system might be significantly degraded. This is precisely the case of direct velocity feedback control (DVFC) with saturation, which has been used for the control of floor vibrations [15]. A proof-mass actuator is used to impart control forces. Although this is positioned at the same location as the sensor (accelerometer with an integration circuit), the resulting root locus map exhibits non-collocated features. More specifically, the actuator dynamics introduce a pair of low-frequency poles that interact with the loci corresponding to the structure dynamics [15,16]. Importantly this might reduce stability margins and cause a significant degradation in the system performance. Moreover, the controlled system could be very sensitive to parameter uncertainties since the control gain should be chosen carefully. In [15], it was shown that a couple of branches in the root locus corresponding to the actuator dynamics go to the right-half plane provoking unstable behaviour in the actuator. A saturation nonlinearity was introduced to avoid this unstable behaviour, but the actuator was then involved in a stable limit cycle (LC) [16], which is not desirable since it could result in dramatic effects on the system performance and its components. Thus, an improvement in the stability of the controlled system, such as the avoidance of LC behaviour, is an interesting issue to deal with.

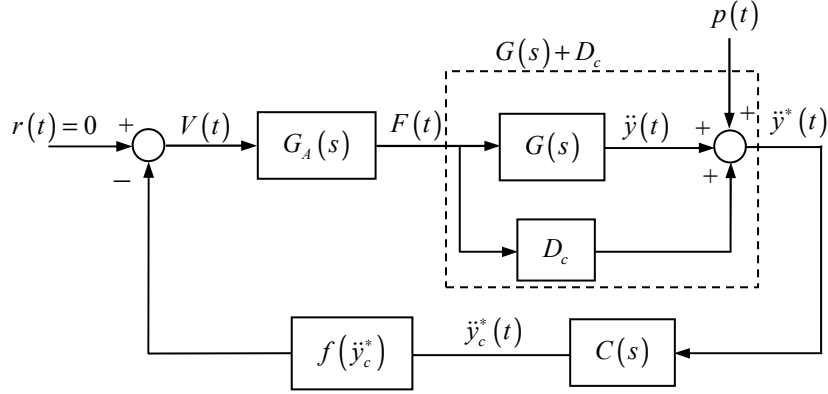
Therefore, this paper proposes the artificial introduction of a direct feed-through term (FTT) in order to transform the non-collocated system features resulting from the use of a proof-mass actuator to collocated system features. A FTT adds a portion of the actuator output signal to the sensor output signal. Typically, the natural frequency of proof-mass actuators used for the control of floor vibrations is chosen to be significantly lower than the lowest natural frequency of floors [16,17]. Taking into account these aspects, a conveniently designed FTT will allow the two zeros located at the origin (product of the acceleration measurement) to be displaced to a position between the actuator poles and floor poles corresponding to its fundamental frequency. Therefore, the resulting controlled system exhibits alternating pole-zero pattern and can be stabilized by a first order compensator. Infinite stability margins are theoretically possible and, in practice, very high gains without exhibiting LC behaviour can be used.

This paper continues with a description of the general control strategy and system dynamics. The influence of proof-mass actuator dynamics on the floor dynamics, the effect of the inclusion of a direct FTT in the AVC system and the design of a feedback compensator are then discussed in Section 3. Simulation and experimental results involving frequency response analyses and walking tests are presented in Section 4 in order to assess the proposed control scheme. Finally, some conclusions are given in Section 5.

2. Control strategy and system dynamics

To design the control system, it is assumed that the actuator dynamics are not affected by the structure dynamics and that the inertial force produced by the actuator is fully applied to the structure. The main components of the general control strategy adopted in this work are shown in figure 1. In this figure, $G_A(s)$ is the transfer function (TF) of the actuator and $G(s)$ is that of the floor structure. The structural acceleration $\ddot{y}(t)$ is measured and a portion of the actuator force $F(t)$ is added to it resulting in a modified acceleration $\ddot{y}^*(t)$. This signal is used by a

feedback compensator $C(s)$. The amount of the actuator force added to the acceleration is imposed by the FTT D_c . The compensator $C(s)$ is designed to allow very high stability margins and to make the system more amenable to the introduction of significant damping by a closed-loop control. The control law is completed by a nonlinear element $f(\ddot{y}_c^*)$ that may be a saturation nonlinearity to account for actuator force overloading [15], an on-off nonlinearity with dead zone [16] or a variable gain with switching-off function [19]. In this work, a saturation nonlinearity will be assumed.



$r(t)$	Reference command	$\ddot{y}(t)$	Acceleration response
$V(t)$	Control voltage	$\ddot{y}^*(t)$	Modified acceleration
$F(t)$	Actuator force	$\ddot{y}_c^*(t)$	Compensated acceleration
$p(t)$	Plant disturbance	$f(\ddot{y}_c^*)$	Nonlinear element
D_c	Feed-through term		
$G_A(s)$	Transfer function of the proof-mass actuator		
$G(s)$	Transfer function of the floor structure		
$C(s)$	Transfer function of the compensator		

Figure 1. General control scheme.

2.1. Floor dynamics

The floor dynamics considering the collocated case between the acceleration (output) and the force (input) and using the modal decomposition approach can be represented in the Laplace-domain as follows [13]

$$G(s) = \sum_{i=1}^n \frac{\alpha_i s^2}{s^2 + 2\zeta_i \omega_i s + \omega_i^2}, \quad (1)$$

in which $s = j\omega$, ω is the frequency, n is the number of considered modes and $\alpha_i \geq 0$, ζ_i and ω_i are the inverse of the modal mass, damping ratio and natural frequency associated with the i^{th} mode, respectively.

2.2. Proof-mass actuator dynamics

A proof-mass actuator generates inertial forces in the structure on which it is placed without the need for a fixed reference. The actuator consists of a reaction (moving) mass attached to a current-carrying coil moving in a magnetic field created by an array of permanent magnets. The moving mass is connected to the frame by a suspension system. Thus, the TF between the

inertial force applied to the structure $F(t)$ and the input voltage $V(t)$ can be closely described as a linear second order system as follows [13]

$$G_A(s) = \frac{K_A s^2}{s^2 + 2\zeta_A \omega_A s + \omega_A^2}, \quad (2)$$

in which $K_A > 0$, ω_A is the natural frequency associated with the suspended moving mass and ζ_A is the damping ratio (including electrical and mechanical effects). The natural frequency ω_A must be sufficiently below the first natural frequency of the structure ω_1 (equation (1)) in such a way that the phase distortion introduced by the proof-mass actuator does not affect significantly the efficacy of the AVC system at the fundamental floor frequency. Typically, it is recommended that ω_A is less than half of ω_1 [20].

3. Controller design

In this section, the effect of the low-frequency dynamics of a proof-mass actuator on the system dynamics is firstly examined. Secondly, the effect of feed-through on the zero dynamics is analyzed and a design criterion for the FTT D_c is proposed. The FTT is selected by an optimization problem in which a functional depending on the phase margin and the maximum potential damping to be added is maximized. Afterwards, the feedback compensator $C(s)$ and the nonlinear element are designed.

3.1. The effect of proof-mass actuator dynamics on system dynamics

It is assumed initially that the actuator has perfect dynamics, which means that it can be modelled by a constant gain. It is also assumed that the measured output is the acceleration, which is the actual magnitude usually measured. The root locus method is used here. The root locus maps the complex linear system roots of the closed-loop TF for control gains from zero (open-loop) to infinity [21]. If a control loop is closed under the two above-mentioned assumptions, the root locus plot is as shown in figure 2a. The system is stable (all the loci remain in the left-half plane) but the loci are narrow and close to the imaginary axis. Therefore, the relative stability (the distance of the roots to the imaginary axis) is poor and the damping is reduced instead of increased (the damping increases as the angle with respect to the negative real axis decreases). Additionally, any unmodelled dynamics will destabilize the closed-loop system. If an integral compensator $C(s) = 1/s$ is applied to the acceleration, the resulting root locus is as shown figure 2b. Hence, the root locus of figure 2b can be interpreted as DVFC. The system exhibits a highly desirable phase margin of 90° and infinite gain margin. The phase plot of the Bode diagram lies between -90° and $+90^\circ$. Furthermore, the relative stability and damping can be increased substantially by the closed-loop control. That is, the system is amenable to the introduction of significant damping by the AVC system.

The actuator dynamics (2) are added to the structure dynamics (1) and direct acceleration feedback is analysed. Figure 3a depicts the root locus obtained in this case. As can be seen, additional dynamics can make the system unstable. As before, an integral compensator leading to DVFC is included in the analysis. The root locus obtained is shown in figure 3b. It can be observed that a couple of branches corresponding to the actuator dynamics go to the right-half plane causing unstable behaviour in the actuator unless low control gains are used. When a saturation nonlinearity is included in the control law, this unstable behaviour is avoided but the actuator might be involved in a stable LC [16]. This lack of stability implies that the control gain has to be chosen carefully. A conservative gain may alternatively be selected although this may not provide the optimum performance of the AVC system.

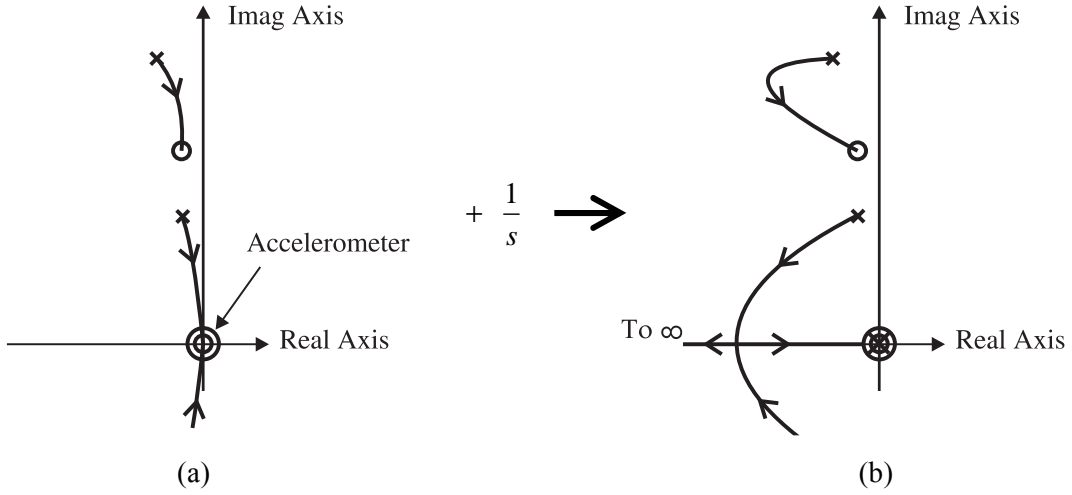


Figure 2. Perfect actuator dynamics case. a) Acceleration feedback. b) Velocity feedback. (x) pole; (o) zero. (Only the upper half of the complex plane is shown, the diagram is symmetrical with respect to the real axis).

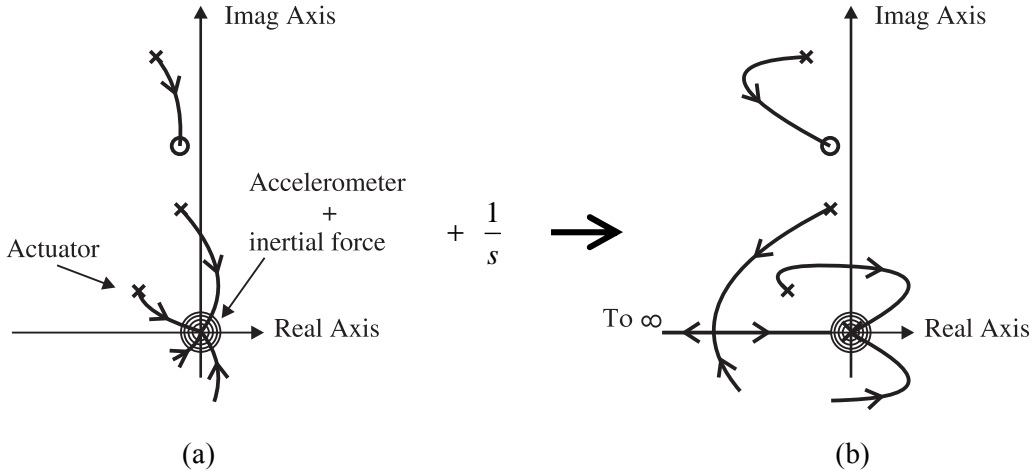


Figure 3. Effect of proof-mass actuator dynamics. a) Acceleration feedback. b) Velocity feedback.

3.2. The effect of feed-through term

The effect of the inclusion of a FTT to the system dynamics is examined here. Zero damping is assumed for the structure dynamics (1) for the sake of simplicity. Aphale et al. [22] demonstrated that the addition of a FTT to the structure displacement (or strain) output introduces a pair of complex conjugate zeros. Here, it is shown that for a system obtained by the sum of n second order subsystems of the form $\alpha_i s^2 / (s^2 + \omega_i^2)$, the addition of a real and positive FTT, D_c , displaces the two zeros at the origin to somewhere in the imaginary axis between the origin and ω_1 .

Theorem: Consider $G(s) = \sum_{i=1}^n \alpha_i s^2 / (s^2 + \omega_i^2)$ such that $\alpha_i \geq 0 \quad \forall i$ and $\omega_1 < \omega_2 < \dots < \omega_n$. If

$\tilde{G}(s) = G(s) + D_c$ with $D_c \in \mathbb{R}^+$, then $\tilde{G}(s)$ can be rewritten as

$\tilde{G}(s) = (s^2 + \omega_z^2) \sum_{i=1}^n \beta_i / (s^2 + \omega_i^2)$ with $\omega_1 > \omega_z$.

Proof: At $s^2 = -\omega_z^2$, $\tilde{G}(s) = 0$, then

$$\tilde{G}(j\omega_z) = \sum_{i=1}^n \frac{-\omega_z^2 \alpha_i}{-\omega_z^2 + \omega_i^2} + D_c = 0 \quad \text{and} \quad D_c = -\sum_{i=1}^n \frac{-\omega_z^2 \alpha_i}{-\omega_z^2 + \omega_i^2}.$$

By the substitution of D_c into $\tilde{G}(s)$, it is obtained

$$\tilde{G}(s) = \sum_{i=1}^n \alpha_i \left(\frac{s^2}{s^2 + \omega_i^2} + \frac{\omega_z^2}{\omega_i^2 - \omega_z^2} \right).$$

By letting $k_i = \omega_z^2 / (\omega_i^2 - \omega_z^2)$ and using that $\omega_z^2 = k_i \omega_i^2 / (1 + k_i)$, $\tilde{G}(s)$ can be written as follows

$$\tilde{G}(s) = \sum_{i=1}^n \alpha_i (1 + k_i) \left(\frac{s^2 + \omega_z^2}{s^2 + \omega_i^2} \right) = (s^2 + \omega_z^2) \sum_{i=1}^n \frac{\beta_i}{s^2 + \omega_i^2},$$

with $\beta_i = \alpha_i \omega_i^2 / (\omega_i^2 - \omega_z^2)$. Note that if $D_c \in \mathbb{R}^+$, then $\omega_1 > \omega_z$ and $\beta_i \geq 0$. This demonstrates that the two zeros will be placed between the origin and ω_1 depending on the value of D_c , which has to be a positive real number.

To show the effect of the FTT, the root locus of the TF of the actuator (equation (2)) and system dynamics (equation (1)) $G_T(s) = G_A(s)G(s)$ is initially considered (figure 4a). As has been demonstrated, the FTT has the effect that the two zeros of the structure at the origin migrate to a particular location (figure 4b). Then, a properly designed FFT will introduce a zero between the actuator and structure poles such that the resulting system will exhibit interlacing of poles and zeros. Thus, the inclusion of an integral action guarantees unconditional asymptotic stability even if the system parameters are subjected to large perturbations (figure 4c). This is because the root locus map keeps the same general shape, and remains within the left half plane when system parameters are changed from their nominal values. Then, the control system is considered to be robust with respect to stability.

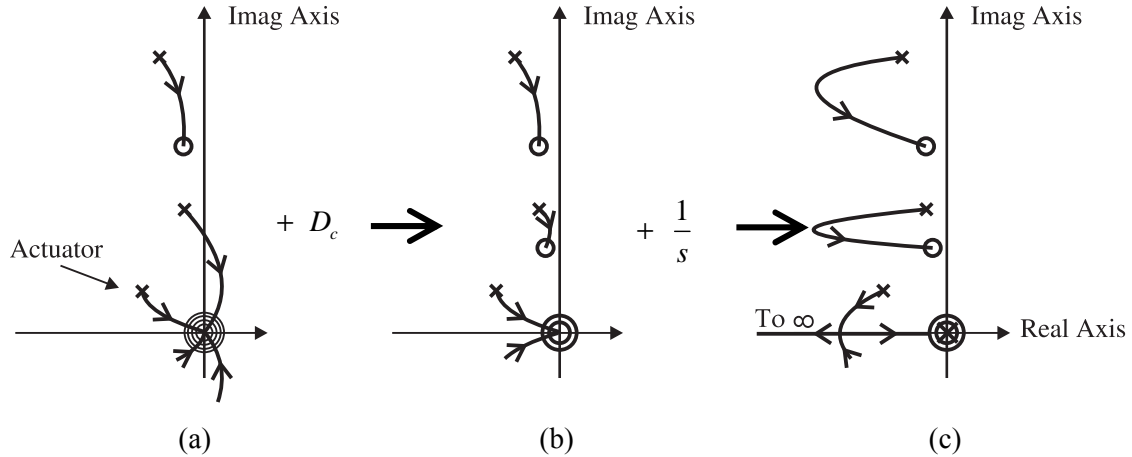


Figure 4. Effect of FTT. a) Acceleration feedback. b) Acceleration feedback + FTT. c) Velocity feedback + FTT.

It is important to note that the phase margin of the control system will be less than 90° since the actuator poles are not close to the imaginary axis. That is, D_c has to be chosen such that the gain margin is infinite and the phase margin is greater than a prescribed safe value (30° for instance). From the root locus, it can be seen that safer values of D_c (higher values) lead to less possible damping to be introduced by the AVC system. Therefore, one should consider this tradeoff in the design of D_c .

3.3. Feed-through term selection

An optimization problem is defined here in order to derive an appropriate value of D_c . The floor TF (1) is considered together with the FTT as shown figure 1. Then, the resulting TF can be written as

$$\tilde{G}(s) = G(s) + D_c = \sum_{i=1}^n \frac{\alpha_i s^2}{s^2 + 2\xi_i \omega_i s + \omega_i^2} + D_c. \quad (3)$$

Thus, the total TF is $G_T(s) = G_A(s)\tilde{G}(s)/s$ in which an integral compensator is added. It is proposed to obtain the FTT by solving the following optimization problem

$$\max_{D_c \in [D_c^{\min}, D_c^{\max}]} \Phi(D_c) = r\hat{\theta}(D_c) + (1-r)\hat{\zeta}(D_c), \quad (4)$$

in which $\hat{\theta}(D_c)$ is the phase margin normalized to 90° and $\hat{\zeta}(D_c)$ is the maximum possible damping to be added by the AVC system for each value D_c normalized by its maximum value, which is achieved for D_c^{\min} . Parameter r is a weighting value to account for the existing tradeoff between the stability and the damping. The normalized phase margin is defined as

$$\hat{\theta}(D_c) = \theta(D_c)/90, \quad (5)$$

with $\theta(D_c)$ (in degrees) defined as

$$\theta(D_c) = 180 - \max \left| \angle G_T(D_c) \right|, \quad (6)$$

in which $\angle G_T(D_c)$ is the phase for each value of D_c . The searching range for the FTT is $D_c \in [D_c^{\min}, D_c^{\max}]$. The lower limit D_c^{\min} is the minimum value of D_c for which $\theta(D_c) \geq \theta^{\min}$, θ^{\min} being the minimum phase margin allowed by the designer. The maximum possible damping is achieved for this value. Then the normalized damping is obtained

$$\hat{\zeta}(D_c) = \zeta(D_c)/\zeta^{\max} \quad \text{with} \quad \zeta^{\max} = \zeta(D_c^{\min}). \quad (7)$$

Finally, D_c^{\max} is the maximum value of D_c such that $\zeta(D_c^{\max}) = \zeta^{\min}$, ζ^{\min} being the minimum damping required by the designer.

3.4. Controller selection

Once the FTT is designed, it is necessary to select the integral compensator $C(s)$ and the nonlinear element $f(\dot{y}_c^*)$ (see figure 1). So far, it has been considered to be a simple integrator $C(s) = 1/s$. However, a DC offset correction is needed in practical implementations and it should be taken into account that a simple integrator leads to unnecessarily high sensitivity at low frequencies. This fact is undesirable since high control inputs at low frequencies might result in actuator saturation without achieving cancelation of the structure vibration modes. Thus, the following controller is proposed

$$C(s) = \frac{s}{s^2 + 2\zeta_c \omega_c s + \omega_c^2}, \quad (8)$$

in which ω_c and ζ_c are, respectively, the natural frequency and damping ratio of the compensator. This controller carries out the magnitude and phase shift of an ideal integrator at frequencies above ω_c whilst it removes the DC offset and avoids unnecessarily high sensitivity at low frequencies. Nonetheless, there is an associated penalty of slightly reduced phase margin. This penalty is negligible if ω_c is chosen to be smaller than ω_A , such as $\omega_c \leq \omega_A/2$.

Finally, the nonlinear element $f(\dot{y}_c^*)$ must be chosen to avoid actuator force and stroke saturation. A saturation nonlinearity is selected

$$f(\dot{y}_c^*(t)) = \begin{cases} K_c \dot{y}_c^*(t) & |\dot{y}_c^*(t)| \leq V_s/K_c \\ V_s \text{sign}(\dot{y}_c^*(t)) & |\dot{y}_c^*(t)| > V_s/K_c \end{cases}, \quad (9)$$

where K_c is the control gain and V_s is the maximum allowable control voltage to the actuator. The control gain K_c is chosen from the root locus method. Loci move from poles to zeros as the gain is increased. Consider figure 4c and focus on the first vibration mode of the structure, the pole moves from close to the imaginary axis increasing its damping until the maximum damping is achieved. Then, higher gain values will reduce the damping. An optimum choice of gain is usually that which maximizes the damping of the fundamental vibration mode of the structure.

The saturation voltage V_s will generally be limited by stroke saturation at the actuator resonance. The saturation affects the system performance so that the gain selected by the root locus method may not be a good choice. Then, numerical simulations are useful to assess the system performance.

3.5. Design process

The design process of the control scheme represented in figure 1 can be summarized in the following steps:

Step 1: Identify the actuator $G_A(s)$ and structure dynamics $G(s)$.

Step 2: Design the FTT D_c by solving the optimization problem defined in Section 3.2.

Step 3: Design a controller $C(s) = s/(s^2 + 2\zeta_c \omega_c s + \omega_c^2)$ by choosing $\omega_c < (\omega_A/2)$.

Step 4: Design the nonlinear element $f(\dot{y}_c^*)$ according to performance (stability is not an issue here). If $f(\dot{y}_c^*)$ is a saturation nonlinearity, take a saturation value V_s to avoid actuator force and stroke saturation and select a suitable gain K_c using the root locus method and/or numerical simulations.

4. Implementation on a laboratory structure

This Section presents the design and implementation of an AVC system based on the procedure presented in Section 3 on a concrete slab strip.

4.1. Experimental setup and system dynamics

The test structure consists of a simply-supported slab strip made of in-situ cast post-tensioned concrete [24]. It has a span of 10.8 m and a total length of 11.2 m, including 0.2 m overhangs over each support. It has a width of 2.0 m, a thickness of 0.275 m and it weighs approximately 15 tonnes. Figure 5 shows photographs of the structure, in which a general view (figure 5a) and a detail of one of the supports (figure 5b) are observed. A single collocated actuator/sensor was placed at mid-span, where the first vibration mode shape has its maximum value.



(a)

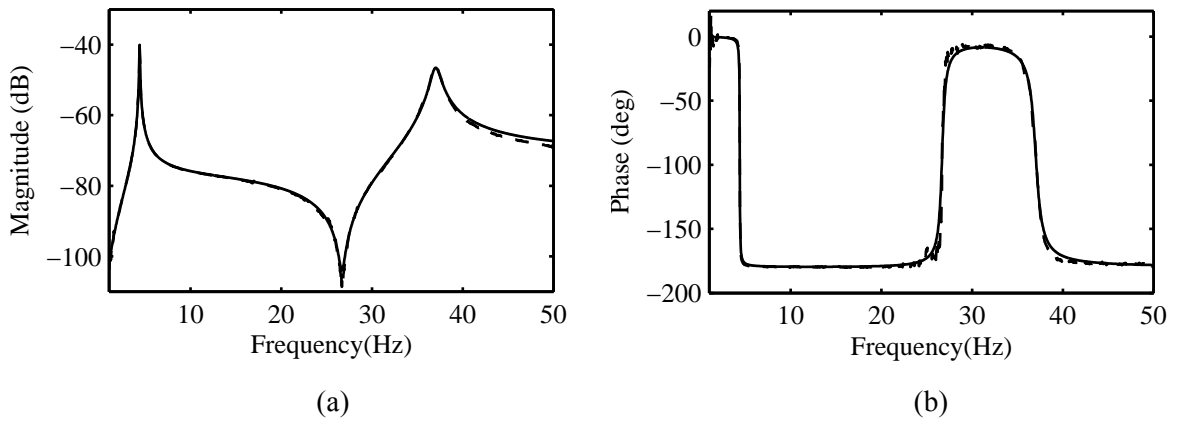
(b)

Figure 5. Photograph of the experimental slab strip. a) General view. b) Simple support and overhang.

The test floor structure was designed in such a way that its first mode (at approximately 4.4Hz) is prone to be excited by the second and third harmonics of walking excitation (pacing frequencies of 1.47 and 2.2 Hz). The Frequency Response Function (FRF) corresponding with the mid-span using a frequency span of 0–50 Hz was obtained experimentally and a posteriori parameter identification of model (1) ($n = 2$) was undertaken

$$G(s) = \frac{1.39 \cdot 10^{-4} s^2}{s^2 + 0.385s + 755.64} + \frac{1.31 \cdot 10^{-4} s^2}{s^2 + 6.509s + 54046}. \quad (10)$$

Figure 6 shows the magnitude and phase responses of the model and experimental floor. The model captures the floor dynamics with sufficient accuracy. Two modes are observed at this location, at 4.44 and 37 Hz. This section will focus on the vibration reduction of the first vibration mode since that is the one that can be excited by normal human activities, such as walking or bouncing.



(a)

(b)

Figure 6. Transfer function of the floor structure $G(s)$: (– –) experimental; (—) model. a) Magnitude in dB referenced to $1(\text{m/s}^2)/\text{N}$. b) Phase in degrees.

The proof-mass actuator used was an APS Dynamics Model 400 electrodynamic shaker (operated in inertial mode) with an inertial mass of 30.4 kg (figure 7a). This actuator was instrumented with a piezoelectric accelerometer (Endevco 7754A-1000) mounted on the inertial mass. The measured acceleration signal multiplied by the magnitude of the inertial mass results

in the inertial force signal applied to the structure ($F(t)$ in figure 1). The actuator model was determined to be

$$G_A(s) = \frac{160s^2}{s^2 + 8.005s + 130.8}. \quad (11)$$

The natural frequency of the actuator is estimated as 11.43 rad/s (1.82 Hz) and the damping ratio $\zeta_A = 0.35$. The peak harmonic force given by the actuator is 320 N (at 10 Hz) and the maximum stroke is 0.158 m.

The floor response was measured using a piezoelectric accelerometer (Endevco 7754A-1000) mounted on a levelled baseplate (figure 7b). The dynamics introduced by the sensor were not considered in the control scheme since they are negligible for the bandwidth of interest. The controller hardware completes the experimental setup. It comprises of a digital computer with a low cost National Instruments PCI-6030E DAQ card installed, which is used to compute digitally the control law.

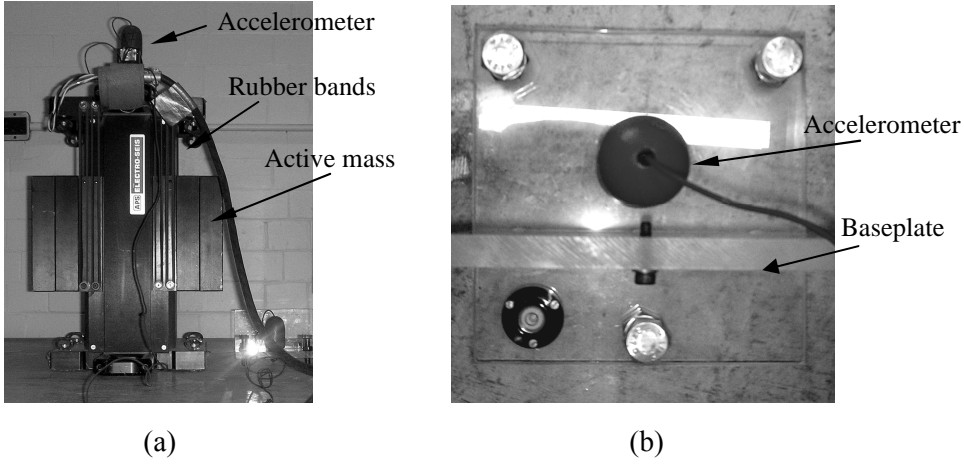


Figure 7. a) Proof-mass electromagnetic shaker (APS Electro-Seis Dynamic Shaker 400) instrumented with an accelerometer. b) Piezoelectric accelerometer (Endevco 7754-1000) mounted on a levelled baseplate (Top view).

4.2. Controller design

The control parameters were obtained following Section 3. As mentioned previously, during real-time control, a digital computer was used for the on-line calculation of the control signal $V(t)$. The system output was sampled with a period $\Delta t = 0.001$ s and the control signal was calculated at each sampling period. Then, the discrete-time control signal was converted into a zero-order-hold continuous-time signal. Likewise, the continuous TF of the compensator was converted to discrete TF using the zero-order-hold approximation.

The FTT was obtained by solving the optimization problem (4). Firstly, a minimum phase margin $\theta^{\min} = 30^\circ$ was chosen. Then, from equation (6), it was obtained that $D_c^{\min} = 4.0 \cdot 10^{-5} \text{ (m/s}^2\text{)}/\text{N}$. Secondly, from equation (7) and assuming $\zeta^{\min} = 0.20$, it was obtained that $D_c^{\max} = 1.47 \cdot 10^{-4} \text{ (m/s}^2\text{)}/\text{N}$. Finally, $\Phi(D_c)$ (equation (4)) was calculated using $r = 0.55$ such that its maximum value was reached for $D_c = 7.78 \cdot 10^{-5} \text{ (m/s}^2\text{)}/\text{N}$. The assumed value of r considers that the stability is more important than the damping.

The feedback controller $C(s)$ (8) was obtained with $\omega_c = 5$ rad/s and $\zeta_c = 0.5$ so that it works as an integrator for frequencies greater than ω_c , yet also simultaneously removes the DC level. The continuous TF of the compensator is as follows

$$C(s) = \frac{s}{s^2 + 5s + 25}. \quad (12)$$

The nonlinear element was chosen to be the saturation nonlinearity defined by equation (9). The saturation value was chosen as $V_s = 0.6 \text{ V}$, which avoids both force and stroke saturation of the actuator for any frequency. The remainder of the section studies the effect of the gain selection when the FTT is included in the control law.

4.3. Frequency responses tests

FRFs were obtained to assess the effect of the FTT on the AVC system performance. It was initially assumed that $D_c = 0$, which is equivalent to DVFC. Figure 8 shows the experimental FRF for gain values $K_c = 0, 100, 300, \dots, 1100 \text{ V/(m/s)}$. A frequency span of 0–10 Hz is shown. Table 1 summarizes the peak amplitude and the vibration reduction for DVFC. The maximum reduction achieved was almost 35 dB and it was observed that the actuator was involved in a stable LC for gains above 700 V/(m/s) . When this occurs, the magnitude of the actuator resonance becomes more important than the structure resonance. This behaviour should be avoided in any practical application.

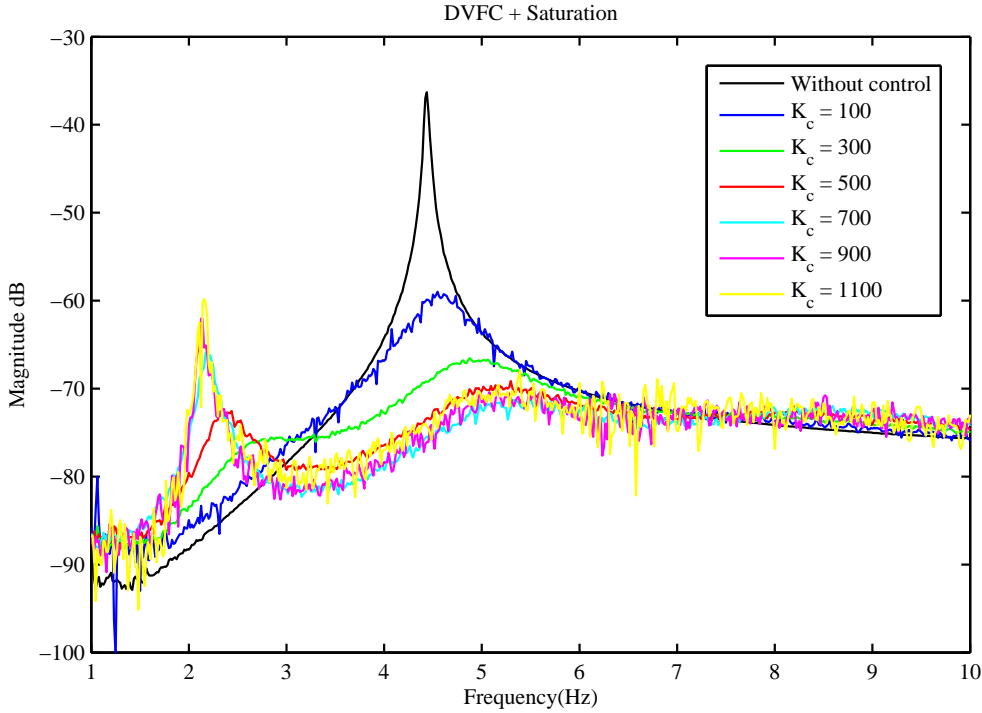


Figure 8. Frequency response tests for DVFC. Magnitude in dB referenced to $1(\text{m/s}^2)/\text{N}$.

Figure 9 shows the experimental FRFs when the FTT is included. Now, very high control gains (up to 1900 V/(m/s)) were used without the observation of LC behaviour. Table 1 shows the peak amplitude and the vibration reduction for each gain utilized. Reductions of up to 40 dB were achieved.

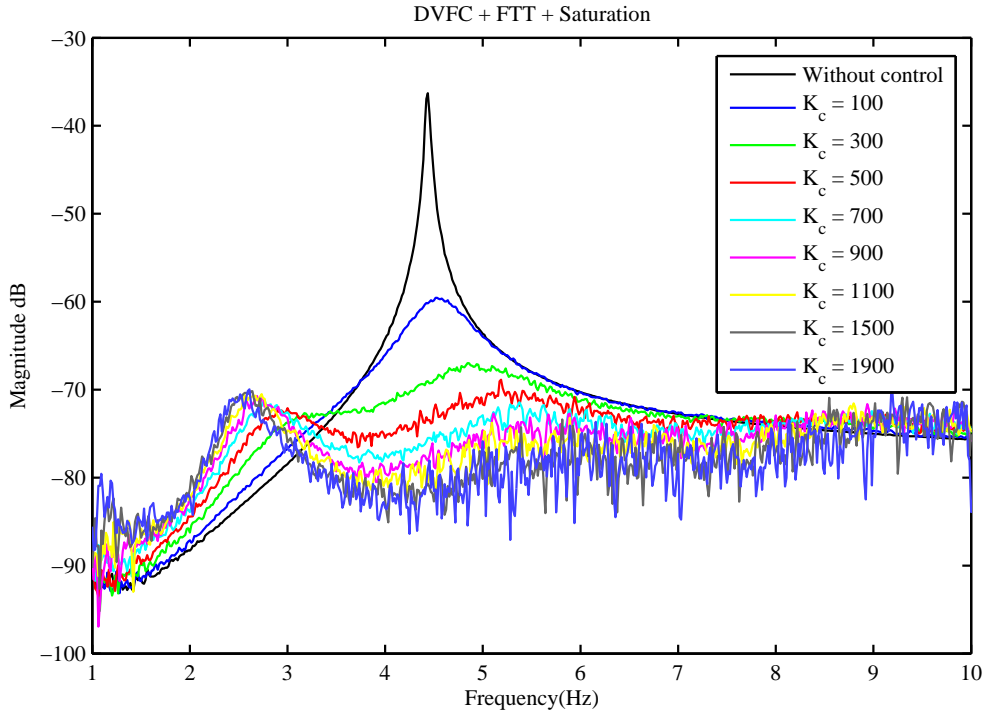


Figure 9. Frequency response tests for DVFC+FTT. Magnitude in dB referenced to $1(\text{m/s}^2)/\text{N}$.

4.4. Walking tests

Walking tests were carried out to assess the AVC system performance when the FTT is included under normal human activities. The same gain scheduling as before was used for DVFC and DVFC+FTT. Two different pacing frequencies (1.48, slow walking, and 2.2 Hz, fast walking) were used in such a way that the first floor vibration mode might be excited by the second or the third harmonic of walking. The results are compared in terms of the maximum transient vibration value (MTVV) calculated from the 1 s running RMS acceleration [25]. Additionally, the BS 6841 W_b weighting function [26] was applied to the response time histories to account for the human sensitivity to vibration at different frequencies. Figure 10 shows one of the walking tests being carried out, which consisted of walking from one end of the slab strip to the other and back again. Each test was repeated three times and the mean value of the MTVV was calculated. The vibration reductions achieved (mean values) are summarized in table 2 for DVFC and when the FTT is included. Vibration reductions of 97 % for slow walking and 88 % for fast walking were observed. Moreover, the FTT avoided the appearance of LC even when very high gains were used. The AVC system was very insensitive to gain selection. Figure 11 shows an example of the BS 6841 W_b weighted acceleration response without control and with control (using $K_c = 1500 \text{ V}/(\text{m/s})$ including the FTT).

5. Conclusions

The active cancellation of floor vibrations induced by human motions has been addressed in this work. A proof-mass actuator working in an inertial mode was used to impart control forces to the floor structure. It has been shown that the inclusion of the actuator dynamics affect drastically the system dynamics even for a collocated control. The interlacing property of poles and zeros is no longer accomplished and the actuator dynamics might become unstable. This makes the AVC system sensitive to parameter uncertainties and the selection of control parameters. This paper has proposed the inclusion of a conveniently designed feed-through term that enables the two zeros at the origin (resulting from acceleration measurement) migrate between actuator and structure poles. An optimization procedure that takes into account stability

and performance simultaneously has been proposed to find the value of the feed-through term. In this way, an integral controller can stabilize the control system. Infinite gain margin and significant phase margin are possible and hence, the AVC system is robust with respect to stability. Thus, the FTT inclusion leads to an AVC system much less sensitive to parameter uncertainties and control parameter selection. Experimental trials conducted on a concrete slab strip have validated and demonstrated the improvements associated with the FTT inclusion. Excellent vibration reduction performance and a high degree of insensitivity to control parameter selection of the AVC system have been reported when the FTT is included.



Figure 10. Walking tests on a concrete slab strip.

Future work should consider an extension of the proposed control strategy to the case of several collocated sensor-actuator pairs. The work of Bhikkaji et al. [27] provides closed-loop stability conditions for the case of multivariable integral control in which a feedthrough matrix is included. This work might be taken into account as an extension of the proposed control strategy.

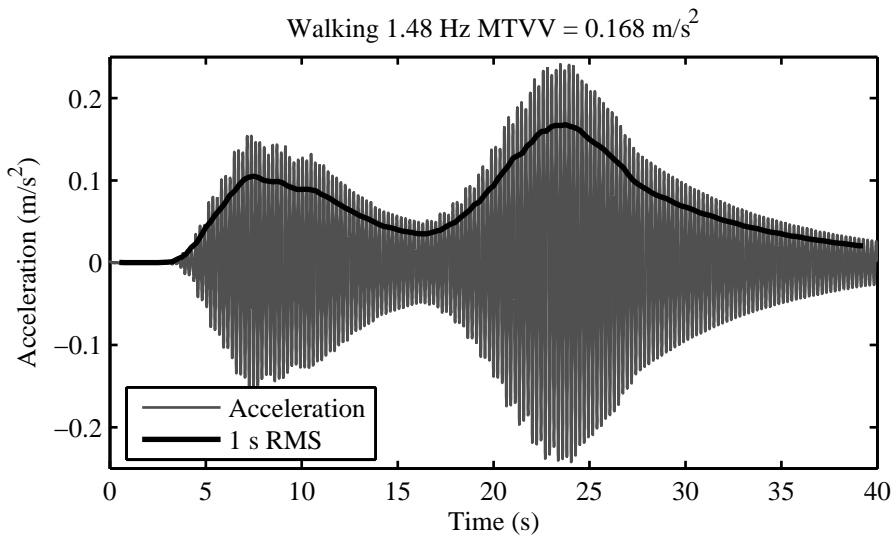
Acknowledgments

The authors would like to acknowledge the financial support of Universidad de Castilla-La Mancha (TC20091110), Conserjería de Educación y Ciencia of Junta de Comunidades de Castilla-La Mancha and European Social Fund. The assistant of Ángel Morales and the suggestions of Emiliano Pereira from Universidad de Castilla-La Mancha are also gratefully acknowledged.

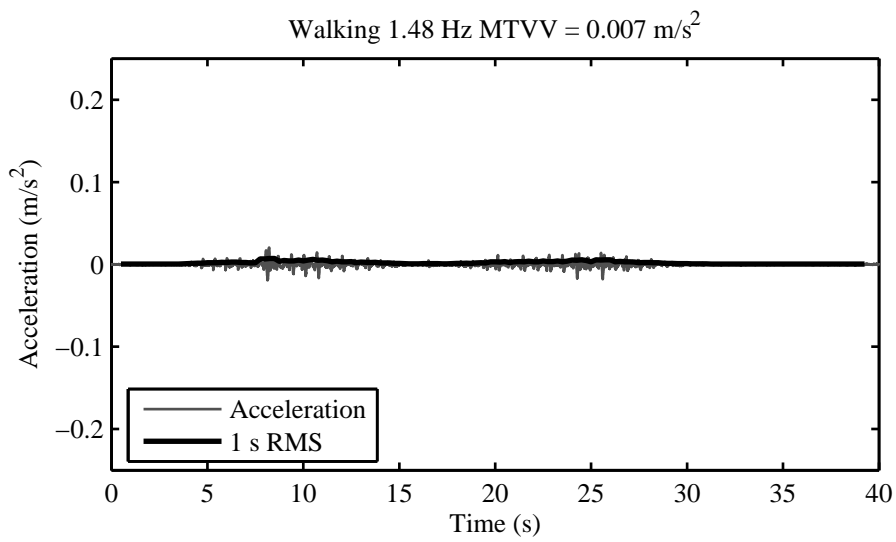
References

- [1] Bachman H 1992 Case studies of structures with man-induced vibrations *J. Struct. Eng.-ASCE* **118**(3) 631–47
- [2] ISO 10137 1992 *Basis for the design of Structures – Serviceability of building against vibration* (International Standards Organization) 41–43
- [3] Murray T M, Allen D E and Ungar E E 1997 Floor vibrations due to human activity *AISC Steel Design Guide* 11, CISC, Chicago, IL
- [4] Setareh M and Hanson R D 1992 Tuned mass damper to control floor vibration from humans *J. Struct. Eng.-ASCE* **118**(3) 741–62
- [5] Setareh M 2002 Floor vibration control using semi-active tuned mass dampers *Can. J. Civ. Eng.* **29**(1) 76–84
- [6] Hanagan L M, Murray T M and Premaratne K 2003 Controlling floor vibration with active and passive devices *Shock & Vibration Digest* **35**(5) 347–65

- [7] Nyawako D and Reynolds P 2007 Technologies for mitigation of human-induced vibration in civil engineering structures *Shock & Vibration Digest* **36**(6) 465–93
- [8] Ebrahimpour A and Sack R L 2005 A review of vibration serviceability criteria for floor structures *Comput. Struct.* **83** 2488–94
- [9] Du H, Zhang N and Nguyen H 2008 Mixed H_2/H_∞ control of tall buildings with reduced-order modelling technique *Struct. Control. Health Monit.* **15** 64–89
- [10] Huo L, Song G, Li H and Grigoriadis K 2008 H_∞ robust control design of active structural vibration suppression using an active mass damper *Smart Mater. Struct.* **17** 1–10
- [11] Wu J C, Chih H H and Chen C H 2006 A robust method for seismic protection of civil frame building *J. Sound Vibr.* **294** 314–28
- [12] Chung L Y and Jin T G 1998 Acceleration feedback control of seismic structures *Eng. Struct.* **20**(1) 62–74
- [13] Preumont A 1997 *Vibration control of active Structures: An introduction* (Dordrecht, The Netherlands: Kluwer Academic)
- [14] Balas M J 1979 Direct velocity feedback control of large space structures *J. Guidance Control* **2**(3) 252–53
- [15] Hanagan L M and Murray T M 1997 Active control for reducing floor vibrations *J. Struct. Eng.-ASCE* **123**(11) 1497–1505
- [16] Diaz I M, Nyawako D S and Reynolds P 2008 On-off nonlinear velocity feedback control for cancelling floor vibrations *Proc. 4th European Conf. on Structural Control* (St. Petersburg, Russia) pp 175–82.
- [17] *APS Instruction Manual Electro-Seis Model 400 Shaker* (USA, APS Dynamics)
- [18] Hanagan L M and Murray T M 1998 Experimental implementation of active control to reduce annoying floor vibrations *Eng. J.* **34**(4) 123–127
- [19] Nyawako D S and Reynolds P 2008 Active control of human induced floor vibrations *Proc. 26th International Modal Analysis Conf.* (Orlando, Florida, USA)
- [20] Hanagan L M 2005 *Active floor vibration system* (United States Patent 6874748)
- [21] Bolton W 1998 *Control engineering* (United Kingdom: Logman)
- [22] Aphale S S, Flemming A J and Mohemani S O R 2007 Integral resonant control of collocated smart structures *Smart Mater. Struct.* **16** 439–446
- [23] Slotine J J, Li W 1991 *Applied non linear control* (Prentice-Hall) Chapter 5
- [24] Reynolds P and Pavic A 2003 Effects of false floor on vibration serviceability of building floors. I: Modal properties *J. Perform. Constr. Facil.* **17** 75–86
- [25] ISO 2631-1 1997 *Mechanical vibration and shock– Evaluation of human exposure to whole-body vibration* (Switzerland: Part 1, General requirement, International Organization for Standardization)
- [26] BS 6841 1987 *Measurement and evaluation of human exposure to whole-body mechanical vibration and repeated shock* (United Kingdom, British Standards Institution)
- [27] Bhikkaji B, Moheimani S O R and Petersen I R 2008 Multivariable integral control of resonant structures *Proc. 47th IEEE Conf. on Decision and Control* (Cancun, Mexico) pp 3743–48.



(a)



(b)

Figure 11. Typical walking time histories ($K_c = 1500 \text{ V}/(\text{m/s})$) including the FFT).

Table 1. Experimental frequency response assessment: 1st vibration mode.

K_c	DVFC			DVFC + FTT		
	Amplitude (dB)	Reduction (dB)	LC ^a	Amplitude (dB)	Reduction (dB)	LC
0	-36.28	—	NO	-36.28	—	NO
100	-58.99	22.71	NO	-59.54	23.26	NO
300	-66.53	30.25	NO	-66.97	30.69	NO
500	-69.75	32.87	NO	-70.24	33.96	NO
700	-71.14	34.86	YES	-72.50	36.22	NO
900	-69.94	33.47	YES	-73	36.72	NO
1100	-67.94	31.66	YES	-75	38.72	NO
1500	—	—	YES	-76	40	NO
1900	—	—	YES	-76	40	NO

^a Limit cycle observation

Table 2. Experimental performance assessment for several control gains and walking excitation.

Walking at 1.48 Hz									
Control gain (V/(m/s))		Uncontrolled	300	500	700	900	1100	1500	1900
DVFC	MTVV ^a (m/s ²)	0.158	0.0014	0.0012	0.009 ^(LC)	0.011 ^(LC)	—	—	—
	Reduction (%)	—	91	92	94	93	—	—	—
FTT	MTVV (m/s ²)	0.158	0.017	0.010	0.011	0.007	0.008	0.007	0.007
	Reduction (%)	—	90	94	94	95	96	97	97
Walking at 2.2 Hz									
DVFC	MTVV (m/s ²)	0.220	0.023	0.026	0.026	—	—	—	—
	Reduction (%)	—	90	88	88	—	—	—	—
FTT	MTVV (m/s ²)	0.220	0.020	0.022	0.024	0.024	0.030	0.026	0.027
	Reduction (%)	—	91	90	89	89	86	88	88

^a Maximum Transient Vibration Value defined as the maximum value of 1s running RMS acceleration